MATERIALS CHEMISTRY
FRONTIERS

REVIEW

View Article Online
View Journal | View Issue

Cite this: *Mater. Chem. Front.*, 2022, **6**, 418

Synthesis and structure design of I–III–VI quantum dots for white light-emitting diodes

Hanxu Lu,†[a] Zhe Hu,†[a] Wenjie Zhou,[a] Jinxin Wei,[a] Wanlu Zhang,*[a] Fengxian Xie*[a] and Ruiqian Guo *[abcd]

Received 28th October 2021,
Accepted 30th December 2021

DOI: 10.1039/d1qm01452h

rsc.li/frontiers-materials

Quantum-dot-based light-emitting diodes (LEDs) have been considered as promising alternatives to traditional light sources due to their photo- and thermal-stability, emission wavelength tunability, and so forth. For the past few decades, I–III–VI quantum dots (QDs) have attracted considerable attention. Compared with binary II–VI or III–V QDs, I–III–VI QDs possess large Stokes shifts, good eco-friendliness and wide tunable emissions covering the visible to the near-infrared region, making them ideal lighting materials. This review summarizes the current research progress of I–III–VI QDs, focusing on the synthesis strategies and structural design. The applications in photoluminescent and electroluminescent white LEDs and improvements in device performances are also reviewed, followed by a discussion on the existing challenges, and the prospect is proposed.

1. Introduction

Over the past decades, quantum dots (QDs) have been widely studied due to their unique optical properties such as controllable fluorescence emission and high color purity.[1–3] They have broad application prospects in solar cells,[4,5] bioimaging,[6,7] photocatalysis,[8,9] and light-emitting diodes (LEDs).[10,11] At present, the II–VI QDs represented by CdSe QDs are up to commercial standards.[12] However, II–VI QDs are inherently toxic because they contain heavy metals like Cd. Although the leakage of heavy metals can be limited by the coating methods,[13] it will inevitably cause harm to the environment, which restricts the large-scale commercial applications of II–VI QDs.

Therefore, it has become an urgent problem for researchers to explore QDs which contain less toxic and more environmentally friendly elements. Over the past few years, InP and other Cd-free QDs have been widely studied. However, due to the narrow emission spectrum, complex synthesis pathway and use of hazardous materials, LEDs based on these QDs have the drawbacks of high price and low efficiency.[14,15] There is a strong desire to develop low-toxicity, highly luminescent QDs with larger Stokes shifts and wider emission spectrum. As rare green materials, I–III–VI (I = Cu, Ag; III = In, Al, Ga; VI = S, Te, Se) QDs have received immense interest from researchers.[16–18] Compared with other Cd-free QDs, I–III–VI QDs have a longer excited-state lifetime, larger Stokes shifts and wider emission spectrum covering the entire visible and NIR window, which can be tuned with their size and composition variations. In addition, these QDs can be synthesized easily, and are environmentally friendly and cost-effective, making them ideal materials for fabricating high-quality white LEDs.[19–21] Since 2004, when the molecular single-source precursor $(PPh_3)_2CuIn(SEt)_4$ was thermally decomposed to form colloidal $CuInS_2$ QDs with a tunable emission peak between 662 nm and 673 nm at 200 °C,[22] many efforts have been devoted to improving photoluminescence quantum yield (PL QY), expanding the tunable range of the spectrum, and exploring optimized synthesis routes.

In this review, we mainly focus on the synthesis, structural design, and LED applications of I–III–VI QDs (Fig. 1). We give an overview of the four main synthesis strategies of I–III–VI QDs, both in the organic and aqueous phase, and introduce their structure with respect to doping, alloying and core–shell. Subsequently, we summarize their applications in white-light-emitting diodes (WLEDs), including photo- and electro-luminescent devices, and introduce the methods to optimize the performance of WLEDs. Finally, we highlight the existing problems and put forward the prospects.

2. Synthesis strategies of I–III–VI QDs

Several routes have been used to synthesize QDs.[23–27] Generally, the synthesis strategies of QDs are categorized either as organic or aqueous synthesis. For alloyed QDs, balancing the reactivity

[a] *Institute for Electric Light Sources, School of Information Science and Technology, Fudan University, Shanghai 200433, China*
[b] *Institute of Future Lighting, Academy for Engineering and Technology, Fudan University, Shanghai 200433, China*
[c] *Zhongshan-Fudan Joint Innovation Center, Zhongshan 528437, China*
[d] *Yiwu Research Institute of Fudan University, Chengbei Road, Yiwu City, Zhejiang 322000, China*
† These authors contributed equally.

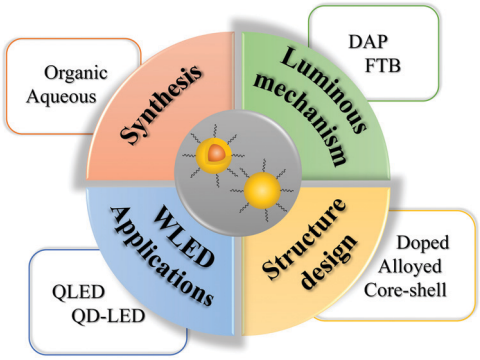

Fig. 1 Schematic presenting the synthesis, luminous mechanism, structural design, and WLED applications of I–III–VI QDs.

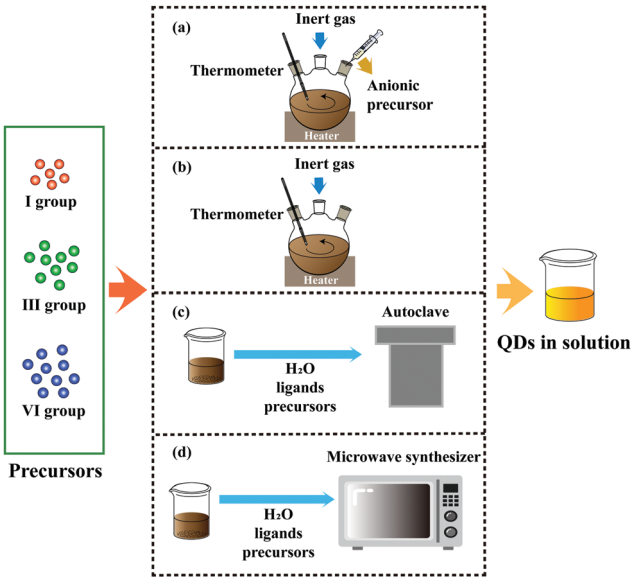

Fig. 2 Four main methods employed to synthesize I–III–VI QDs: (a) hot injection, (b) heating up, (c) hydrothermal and (d) microwave-assisted.

of the constituent precursors is the crucial point for both aqueous and organic routes. According to the Hard-Soft-Acid–Base (HSAB) theory proposed by Pearson in 1963,[28] reactants can be categorized as acids or bases according to their tendency to either accept or donate electrons. Hard acids prefer to bind hard bases and soft acids prefer soft bases, which is the key to synthesizing single-phase and stable alloyed QDs. Group I and group III metals are usually soft and hard acids, and chalcogen anions are usually soft bases. Because of this imbalanced reactivity, two or more ligands are usually selected to increase or decrease the reactivity, respectively, so that they can match each other and avoid the formation of binary QDs.[29,30] Mercaptan, amine, and carboxylic acid are often used in organic synthesis, while glutathione, cysteine, and sodium citrate are often used in aqueous synthesis.[31]

Most I–III–VI alloyed QDs synthesized in the organic phase have good dispersion and excellent optical properties because the organic synthesis can provide a higher reaction temperature. Thus, QDs synthesized in the organic phase have a better crystallinity and a relatively high PL QY.[32,33] However, organic synthesis requires high temperature, inert atmosphere protection, and a relatively complex operation. Furthermore, QDs synthesized in the organic phase are oil-soluble, which limits their biological applications. Although it is possible to change the hydrophobic surfaces of QDs to hydrophilic surfaces by means of ligand exchange, the luminescence properties of the resulting QDs will be greatly reduced.[34–36]

Aqueous synthesis can effectively solve the problems above with the advantages of simple operation, environmental protection, and low cost. However, compared with organic synthesis, the low reaction temperature leads to some prominent problems, such as low PL QY and a narrow adjustable range of the emission peak. A brief discussion of four main methods has been provided in this section (Fig. 2).

2.1 Organic synthesis

2.1.1 Hot injection method. In the hot injection method, the cationic precursors and surfactants react at a certain temperature, and then the anionic precursor is rapidly injected into the hot solution which leads to immediate supersaturation. The aggregation of precursors induces rapid nucleation and the attained QDs have good monodispersity. In 1993, Murray *et al.*[37] used the hot injection method to synthesize CdE (E = S, Se, Te) QDs for the first time. Subsequently, this method has been widely used in the synthesis of I–III–VI QDs. Jong *et al.*[38] successfully prepared highly bright, white-emitting CuGaS/ZnS (CGS/ZnS) QDs with various stoichiometries. With the decrease in Cu/Ga ratio, the absorption peaks showed a blue-shift and the PL QY increased from 26% to 73%. When Cu/Ga = 1/8, the QDs gave a pure white emission with the wide emission covering blue to red. Bing *et al.*[39] synthesized green-emission multi-layer CuInS/ZnS (CIS/ZnS) QDs with a maximum PL QY of ~85% at the peak wavelength of ~530 nm *via* the hot injection method at a low temperature (~130 °C). They chose S-OAm (S powder dissolved in oleamine) as a sulfur source instead of 1-dodecanethiol, which supplied a high concentration of H_2S, leading to the explosive nucleation of CIS QDs (Fig. 3a). The rapid nucleation led to a smaller size of CIS QDs, whose bandgap was wider than CIS QDs using 1-dodecanethiol as a sulfur source (DDT-CIS). By increasing the coating layers of ZnS, the PL emission peaks blue-shifted (Fig. 3b and c), which attributed to the formation of an alloy interface of ZnCuInS (ZCIS) and ZnS shells.

2.1.2 Heating up method. The heating up method is suitable for the large-scale preparation of I–III–VI QDs. This method usually consists of dissolving the precursors, such as metal salts and ligands, in a pot and then directly heating it at a specific temperature for a period. The metal salts are decomposed and undergo the crystallization process in the presence of surfactant and high boiling point solvents. Mei *et al.*[40] reported the utilization of the heating up method for the synthesis of CuGaSe/ZnSe QDs (Fig. 4). They used octadecene as the solvent, and oleamine and 1-dodecanethiol as the ligands. By adjusting the Se/S ratio and Cu/Ga ratio, the emission peak could be continuously adjusted between 485–630 nm and the PL QY could reach 77%. Huang *et al.*[41] synthesized CIS/ZnS QDs in the dispersion state

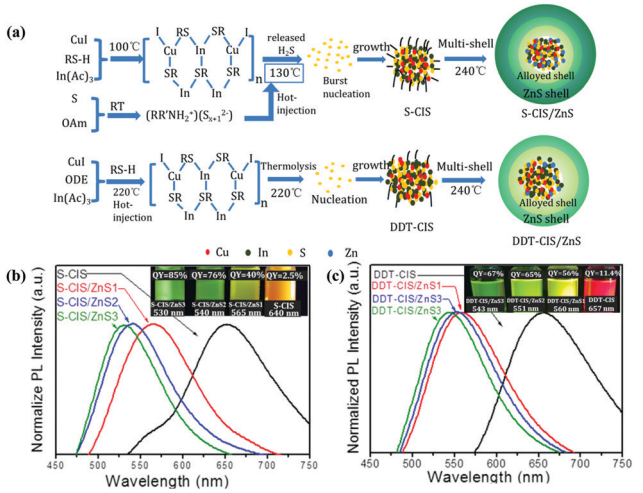

Fig. 3 (a) Schematic illustration of the formation process of CIS/ZnS QDs with S-OAm (S-CIS/ZnS) and 1-dodecanethiol (DDT-CIS/ZnS) as the sulfur source. Normalized PL emission spectra and photographs of the samples under 365 nm UV illumination (inset) of (b) S-CIS/ZnS and (c) DDT-CIS/ZnS QDs. Reproduced with permission.[39] Copyright 2020 Published by Elsevier B.V.

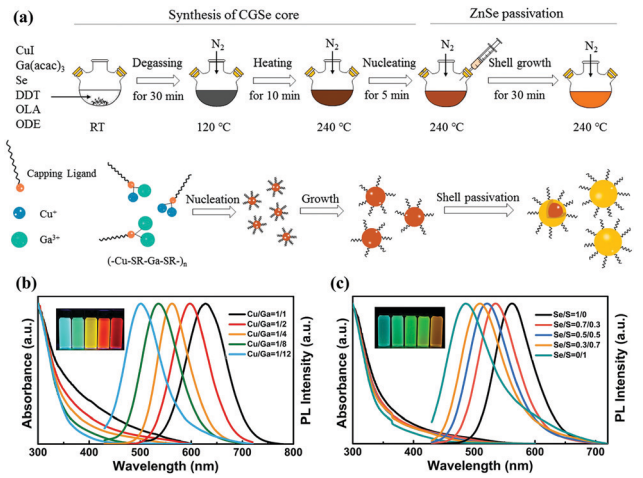

Fig. 4 (a) Schematic illustration of the synthetic procedures of CuGaSe/ZnSe core/shell QDs *via* a heating-up method. UV-vis absorption (left), PL spectra (right, λ_{ex} = 405 nm) and digital photograph of samples under the radiation of 365 nm UV illumination (inset) of (b) CuGaSe/ZnSe and (c) $CuGaSe_xS_{1-x}$/ZnSeS QDs prepared under various Cu/Ga and Se/S precursor molar ratios, respectively. Reproduced with permission.[40] Copyright 2018 Elsevier B.V. All rights reserved.

belonging to the NIR-I window with a PL peak wavelength of 816 nm and FWHM of about 246 nm. With fast precursor decomposition leading to monomer conversion improvement, the PL QY was up to 94.8%.

2.2 Aqueous synthesis

2.2.1 Hydrothermal method. Aqueous synthesis has drawn tremendous interest due to its non-toxic, low cost, and good biocompatibility. Metal nitrate or metal halides are often used as metal precursors while Na_2S or thiourea ($CS(NH_2)_2$) is mostly

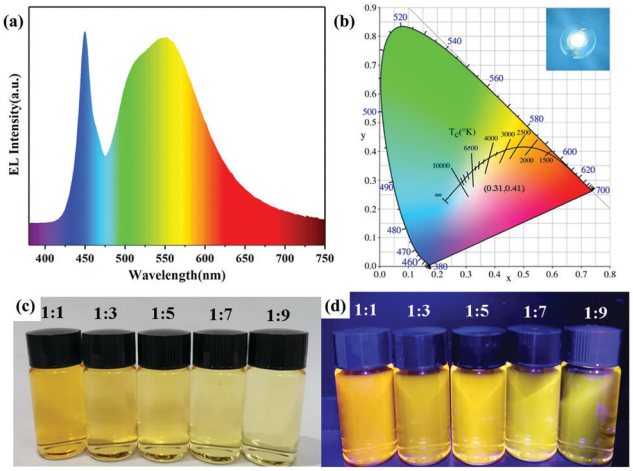

Fig. 5 (a) Electroluminescent (EL) spectrum, (b) the corresponding Commission Internationale de l'Eclairage (CIE) color coordinates and a photograph (inset) of the WLED operating at 50 mA. Photographs of AIZS QDs with different Ag/In ratios under (c) daylight and (d) UV light. Copied with permission.[42] Copyright 2020 Elsevier B.V. All rights reserved.

used as a sulfur source. Chen *et al.*[42] reported the synthesis of water-soluble AgInZnS (AIZS) QDs *via* a hydrothermal method with the assistance of N-methylimidazolium tetrafluoroborate ([Mim]BF_4). In this approach, [Mim]BF_4 was added as the surfactant while glutathione (GSH) and trisodium citrate were employed as ligands. By varying the amount of [Mim]BF_4, the reaction temperature, and cation ratios, AIZS QDs were attained with a PL QY up to 28.9% and an emission peak adjusted from 608 nm to 525 nm. By combining AIZS QDs and green $Lu_3Al_5O_{12}:Ce^{3+}$ phosphors with a blue InGaN chip, a WLED was fabricated (Fig. 5), whose luminous efficacy (LE) reached 85.2 lm W^{-1}.

2.2.2 Microwave-assisted method. The microwave-assisted method based on aqueous synthesis not only has the advantages of environmental friendliness and high reproducibility, but also reduces the reaction time.[43] Furthermore, the microwave-assisted method can rapidly and homogeneously raise the temperature, which reduces the possibility of sharp thermal gradients in reaction conditions, resulting in more uniform nucleation and particle growth. Soares *et al.*[44] synthesized AgInS/ZnS (AIS/ZnS) QDs with a PL QY up to 60% and emission peak adjusted from 630 nm to 700 nm *via* a microwave-assisted method. By systematically assessing synthetic parameters including reaction time, temperature, Ag : In ratio, MPA : In ratio, pH, and so on, they modelled the correlation between the different synthetic parameters and the optical properties (Fig. 6). The model could be used to predict different outcomes of the reactions and then be validated by new experiments. This model could direct the synthesis and pave the way for a deeper understanding of the fundamental properties of I–III–VI QDs.

3. Luminous mechanism of I–III–VI QDs

Compared with other QDs such as CdSe or InP QDs, I–III–VI QDs have a longer PL lifetime, larger Stokes shifts, and wider full-width at half-maximum (FWHM).[45–48] It is widely accepted

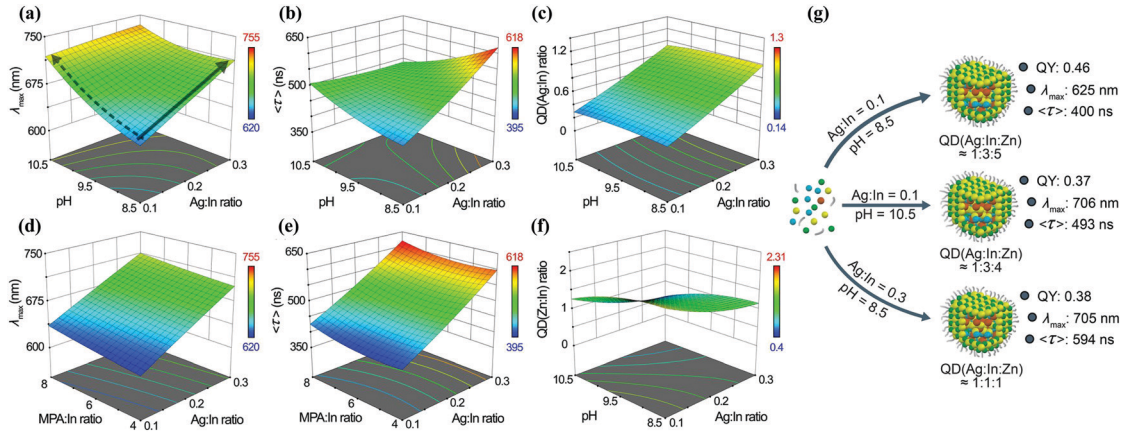

Fig. 6 The relationship between pH, Ag : In ratio, and (a) λ_{max}, (b) $\langle\tau\rangle$, (c) QD (Ag : In) ratio and (f) QD (Zn : In) ratio, when the MPA : In ratio is fixed at 8. The relationship between MPA : In ratio, Ag : In ratio, and (d) λ_{max} and (e) $\langle\tau\rangle$, when the pH is fixed at 8.5. (g) The relationship between the experimental conditions used for AIS/ZnS QD synthesis and their PL properties; the MPA : In ratio was set to 6 for all the designed QDs. QD (Ag : In : Zn) refers to the Ag : In : Zn ratio effectively found in the prepared QDs. Reproduced with permission.[44]

that the former two optical properties are derived from the defect state levels, while the wider FWHM is caused by the variations of size and composition of QDs.[49] At present, the luminous mechanism of I–III–VI QDs is controversial, and two models for radiative recombination have been proposed.[50]

3.1 Donor–acceptor pair (DAP) recombination

DAP recombination (Fig. 7a) involves the bonding between a delocalized donor state electron and a hole localized in the acceptor level. In the case of CIS QDs,[51] defects arising from the nonstoichiometric composition are mainly sulfur vacancies (V_S), copper vacancies (V_{Cu}), and copper indium substitution (In_{Cu}) because Cu–S binding is weaker than In–S binding. V_S and In_{Cu} are believed to be the donor state, whereas V_{Cu} acts as acceptors. Chen *et al.*[52] demonstrated that the optical properties of CIS QDs could be significantly influenced by stoichiometry control. There is no fluorescence in Cu-rich CIS QDs after the Cu/In ratio exceeds a certain value. Most of the luminescent CIS samples are in the copper-deficient region, which suggests the DAP mechanism.

3.2 Free-to-bound (FTB) recombination

FTB recombination (Fig. 7b) implies recombination of a delocalized conduction band (CB) electron with a hole localized at the defect. Zang *et al.*[53] found that a single CIS QD with a thick ZnS shell displayed a narrower photoluminescence line width (down to ~60 meV) than the ensemble (typically >300 meV) and concluded that the photoluminescence in CIS QDs arose from radiative recombination of a delocalized band-edge electron and a localized hole residing on a Cu-related defect. Stam *et al.*[54] held that Cu^{2+} states resulted in individual 'dark' QDs, whereas Cu^{+} states resulted in 'bright' QDs. They proposed that efficient hole trapping on Cu^{+} defects was crucial for 'bright' CIS QDs, and injecting electrons into the 'dark' defect states (Cu^{2+}) could activate efficient hole trapping, which contributed to the control of optical properties.

There were also suggestions that the DAP and FTB mechanisms coexisted as competitive recombination in QDs, while the dominant recombination was determined by the stoichiometry and structure of QDs.[55] Other reasonable hypotheses can be proposed, and more experiments are needed to verify the luminous mechanism of I–III–VI QDs.

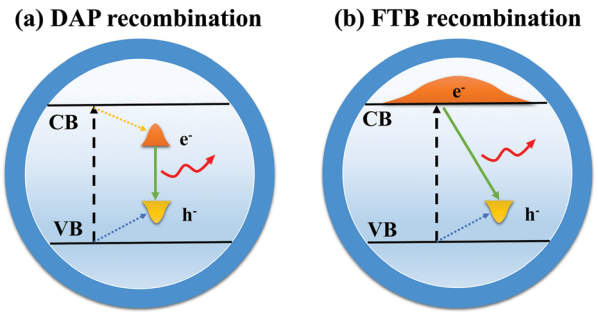

Fig. 7 Schematic representation of the (a) DAP recombination and (b) FTB recombination.

4. Structural design of I–III–VI QDs

4.1 Doped structure

The luminous mechanisms mentioned before are all caused by internal defects. Therefore, the group I-deficient strategy (with reduced Cu/In or Ag/In ratio) can improve the recombination rate of carriers and significantly improve the luminescence intensity of QDs.[56–59] In addition, doping strategies have also been used to enhance the fluorescence and broaden the spectrum of QDs.

Doping in I–III–VI QDs is an important aspect. Doped atoms or ions as external impurities create local quantum states within the bandgaps, and modulate photoluminescence. Kim and coworkers[60] synthesized Mn-doped CGS/ZnS QDs possessing a high PL QY in the range of 74–76% regardless of Mn concentration. These doped QDs with wide PL coverage of green-to-red were packaged as single downconverters with a

blue LED chip to fabricate solid-state lighting devices. Li *et al.*[61] synthesized quaternary CuZnGaSe QDs and quinary CuMnZnGaSe QDs. The white-emission CuMnZnGaSe QDs are promising light-emitting materials suitable for solid-state lighting.

4.2 Alloyed structure

The bandgap of QDs can be tuned by adjusting their size. The synthesis of size-controlled QDs has been extensively studied.[62–64] In many specific applications, very small QDs are needed to obtain the desired properties. However, particles with very small diameters (<2 nm) are unstable.[65] Therefore, a size-independent method to tune the bandgap of QDs is required.

Alloying is a strategy to tune the bandgap of QDs. The desired alloyed QDs are obtained by cation or anion exchange based on a semiconductor material. Hu *et al.*[66] successfully synthesized $Cu_xAg_{1-x}InSe_2$ alloyed QDs through the cation exchange reaction starting from $AgInSe_2$ QDs. With the increase in copper content, the PL emission gradually shifted from 706 to 840 nm, which determined the bandgap evolution of the $Cu_xAg_{1-x}InSe_2$ alloyed QDs. Bai *et al.*[67] prepared alloyed $AgIn(S_{1-x}Se_x)_2$ QDs from $AgInSe_2$ QDs. With the decrease in Se content, the bandgaps could be continuously tuned from 1.45 eV to 1.99 eV.

It should be noted that alloying and doping are different strategies. Though doping and alloying are both carried out through ion exchange, doping does not shift the bandgap of the host nanocrystals but modifies the band structure by creating local quantum states within the bandgaps. When the number of ions exchanged reaches a certain range, an alloyed structure is formed and the bandgaps of QDs are tuned.

4.3 Core–shell structure

Due to the high surface-to-volume ratio of QDs, many surface defects act as temporary 'traps' for the electron, hole, or excitons, quenching radiative recombination and reducing the PL QY. An important strategy to passivate their surface is the overgrowth of a shell consisting of a second semiconductor with a larger bandgap, such as ZnS[68] and CdS,[69] resulting in a core–shell structure. Yoon *et al.*[70] implemented an Al-doped ZnS shell on CIS QDs, resulting in exceptional photostability with a marginal loss of 10% even after a much-prolonged time of 120 h under prolonged UV irradiation exposure and an exceptionally high PL QY up to 90%. Opposite to the ZnS shelling of traditional CdSe QDs,[71] in most cases, ZnS shelling of I–III–VI QDs leads to blue-shifts in both the absorption and photoluminescence spectra. These blue-shifts result from a complex interplay between several processes, including cation exchange,[72] etching,[73] alloying[74] and shell overgrowth.[75] Berends *et al.*[76] addressed that low reaction temperatures (150 °C) favored etching, cation exchange, and alloying, regardless of the precursors used, and ZnS shell overgrowth only became dominant if reactive S- and Zn-precursors and high reaction temperatures were used. Different from alloyed structures, the core–shell structure is carried out through the epitaxial overgrowth of a second semiconductor on the surface of the QDs, which does not change the bandgap of the QDs. However, in most cases, the shell coating and alloying processes occur simultaneously, forming a core/gradient alloy/shell structure.[77,78] A delicate balance between several processes determines the outcome of shelling reactions on QDs. It is not easy to distinguish between a core–shell structure and an alloyed structure after the shelling process. The complex composition brings various properties to I–III–VI QDs, which need further study.

5. Applications of I–III–VI QDs in WLEDs

Due to their durability, high efficiency, energy-saving, and other advantages, LEDs have drawn much attention in laboratories and industries. QDs can not only be employed as conversion materials in photoluminescent WLEDs, but can also be excited electrically to generate white light.[79,80] Therefore, QDs can be applied to manufacture a new generation of lighting devices, which show broad application prospects in the lighting field.

5.1 Photoluminescent WLEDs based on I–III–VI QDs (QD-WLEDs)

In photoluminescent WLEDs, conversion materials absorb the excitation light and re-emit light at longer wavelengths, which mix with the unabsorbed excitation light to form white light. Current commercial WLEDs are mainly based on blue InGaN chips and yellow YAG:Ce phosphors. Due to the narrow emission spectrum of YAG:Ce phosphor, which lacks the emission of the red band, the color rendering index (CRI) of such devices is generally low. Conversion materials with the properties of large Stokes shifts, high PL QYs, reasonable photochemical and thermal stability, strong absorption of UV or blue light, and wide emission bandwidth can be used to obtain white light with high LE and CRI. I–III–VI QDs possess most of these desirable characteristics, which can be employed as conversion materials in photoluminescent WLEDs.

5.1.1 QD-WLEDs based on combinations of I–III–VI QDs and phosphors. When CIS QD-based WLEDs were first reported, the CRI was lower than 80,[81] failing to meet with the standard of indoor lighting. One solution is to mix QDs with conventional phosphors. Li *et al.*[82] prepared CIS/ZnS QDs with PL QYs up to 85% and an emission peak adjusted from 651 nm to 775 nm *via* simple solvothermal synthesis. WLEDs with CRI up to 90 were fabricated using CIS/ZnS QDs and $(Ba,Sr)_2SiO_4:Eu^{2+}$ as color converters in combination with blue LED chips. Chen *et al.*[83] synthesized water-soluble yellow-orange emission AIS/ZnS QDs with PL QYs up to 45.7% *via* the hydrothermal method. By combining a blue InGaN LED chip with a mixture of the AIS/ZnS QDs and $Lu_3Al_5O_{12}:Ce^{3+}$ phosphors, bright white light was successfully generated. The WLED exhibited a high LE of 77.98 lm W^{-1} and a CRI of 85 (Fig. 8).

5.1.2 QD-WLEDs based on combinations of two QDs. Compared to phosphors, the nanoscale size of QDs makes them easier to disperse in polymer matrices. It is easy for QDs to deposit uniform films, reducing the effects of scattering, reflection, and refraction.[84] Su *et al.*[85] synthesized AIS/ZnS QDs whose PL emission can be tuned from 540 to 622 nm by simply

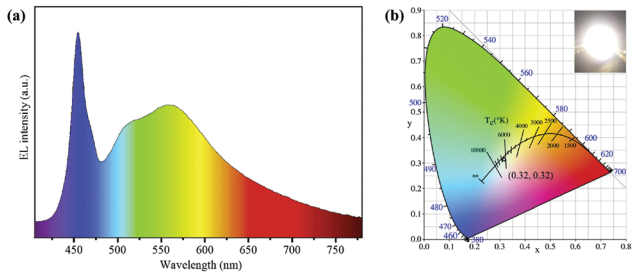

Fig. 8 (a) EL emissive spectra of a WLED fabricated by the green $Lu_3Al_5O_{12}:Ce^{3+}$ phosphors and yellow-emissive AIS/ZnS core/shell QDs, and (b) the corresponding CIE color coordinates of WLED and a photograph of the device operated at 200 mA (inset). Copied with permission.[83]

varying the Ag/In ratio and embedding them in a polyacrylamide hydrogel to fabricate a composite film (Fig. 9). They combined the films with blue LED chips for the fabrication of remote-type warm WLEDs. The WLED based on a yellow composite film displayed white light emission with a CRI of 75.6, while the WLED fabricated by stacking a green film on a red film possessed a relatively high CRI of 87.5. Kim and coworkers[86] synthesized green emissive CGS and red emissive CIS QDs, with PL QYs of 85% and 83%, respectively. These two QD emitters were co-packaged in blue LED chips for the fabrication of tricolored WLEDs. By varying the weight ratio of the two QDs loaded, the as-prepared WLEDs possess exceptional CRIs of 94–97 along with high LEs of 43.1–68.8 lm W^{-1}.

5.1.3 QD-WLEDs based on single-component I–III–VI QDs. Although combining different kinds of QDs can achieve a high CRI, it not only enhances the reabsorption between different QDs which may reduce the LE, but also makes the packaging process more complicated and expensive. Besides, the as-prepared devices indispensably exhibited an undesirable spectral variation with the luminescence intensity of each emitting component changing with the chip current. These issues could be overcome by employing single-type QDs. Kim *et al.*[60] reported the synthesis of white-emitting Mn^{2+} doped CGS/ZnS QDs. They combined QDs with different Mn concentrations with blue LED chips as single downconverters for the fabrication of WLEDs (Fig. 10). WLED with an exceptional CRI up to 95 and a LE of 34.5 lm W^{-1} was attainable when Mn/Ga = 1.25. Gugula *et al.*[87] synthesized ZnCuInGaS QDs with a PL QY up to 82% and a large Stokes shift which could limit or even eliminate reabsorption. By 1-step or 2-step annealing, QDs emitting white light directly (WQDs) or featuring a 'candle-like' orange photoluminescence (CQDs) were attained. The emission spectra of these quinary QDs covered from blue to red, which enabled the fabrication of single-component QD-WLEDs. The WLED composed of a blue LED chip and WQDs boasted a CRI up to 96, while the CQD-based device presented a high LE of 43 lm W^{-1} and a CRI of 93.

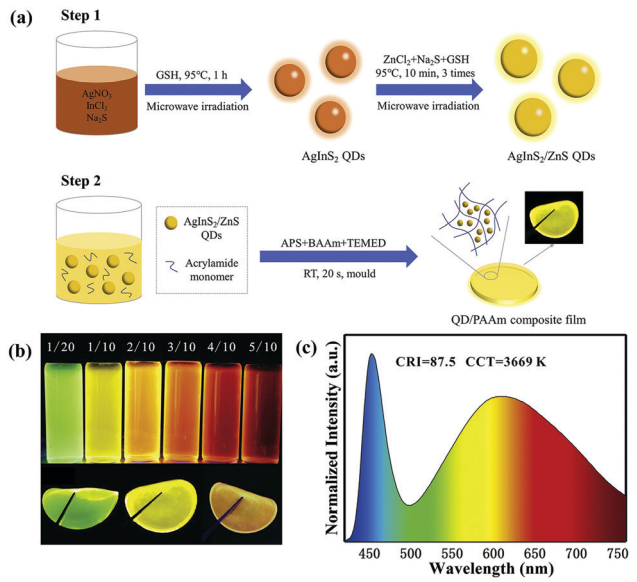

Fig. 9 (a) Synthetic illustration for the preparation of AIS/ZnS QDs and QD/PAAm composite film for WLEDs. (b) Digital photographs of AIS/ZnS QDs synthesized at different molar ratios of Ag/In (above) and QD/PAAm composite films of green, yellow, and red (below) under UV irradiation. (c) Emission spectrum of the LED based on both green and red QD/PAAm films at a drive current of 20 mA. Reproduced with permission.[85] Copyright 2020 Elsevier B.V. All rights reserved.

5.2 Electroluminescent WLEDs based on I–III–VI QDs

QDs have the advantages of tunable emission spectra, high efficiency, and excellent color purity. They can be integrated into electrically-driven quantum-dot light-emitting diodes (QLEDs) after simple solution processing such as spin coating or ink-jet printing. QLEDs operate *via* direct charge carrier injection into the QD layer, which helps us take full advantage of the solution processability of QDs to achieve large-area LEDs. Due to the inherent broad emission bandwidth, I–III–VI QDs are not suitable for displays that require a high degree of color saturation. However, they are ideal materials for solid-state lighting devices, where QDs with a wide PL spectrum are preferred to attain high CRI.

5.2.1 Core/shell structure engineering. QLEDs operate *via* radiative recombination of excitons formed by electrons and holes injected into the QDs. Therefore, the non-radiative recombination caused by Auger recombination (AR) and Förster resonant energy transfer (FRET) will seriously affect the photoelectric performance of EL devices.[88–90] The formation of an alloyed or compositionally graded intermediate layer at the core–shell interface has been proven to be useful to suppress that process.[91] Beyond that, the shell thickness of QDs shows a great effect on device efficiency. Kim *et al.*[92] prepared QLEDs with the structure of ITO//PEDOT:PSS//PVK//CIS/ZnS QDs//ZnO//Al. Through different shelling periods, CIS/ZnS QDs with different degrees of alloying and shell thickness were synthesized. They showed that with an increasing degree of alloying and a thicker shell, nonradiative AR and FRET processes were suppressed more effectively. QLEDs with an unprecedentedly high current efficiency (CE) of 18.2 cd A^{-1} and EQE of 7.3% were attained based on the QDs with the thickest shell. Subsequently, they fabricated QLEDs using Mn-doped ZCGS QDs double-shelled with ZnS.[93] The PL QY of double-shelled QDs was enhanced to 76%. Changes in Mn concentrations resulted

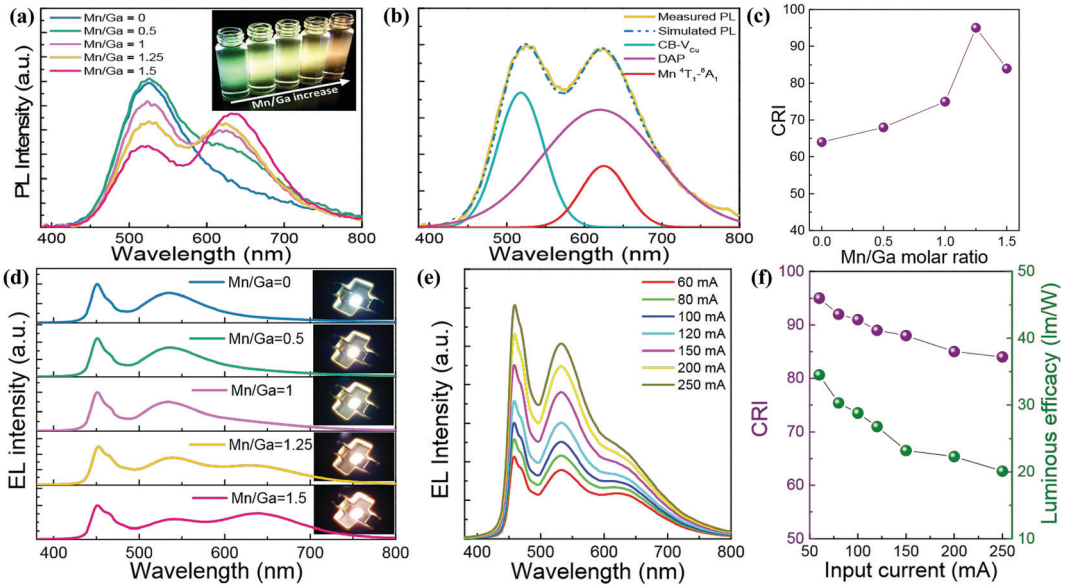

Fig. 10 (a) PL spectra and UV-irradiated fluorescent image (inset) of a series of Mn^{2+} doped CGS/ZnS (Mn:CGS/ZnS) QDs with different Mn/Ga ratios. (b) PL spectral decomposition result of Mn/Ga = 1.25-based Mn:CGS/ZnS QDs. (c) CRI and (d) EL spectra of 60 mA driving WLEDs packaged with Mn:CGS/ZnS QD downconverters with different Mn concentrations. Input current-dependent (e) EL spectra and (f) CRI-LE of Mn/Ga = 1.25-based WLED. Reproduced with permission.[60] Copyright 2018 Optical Society of America.

in tunable PL from bluish, white, to reddish white. When Mn/Cu = 16, QLEDs with a maximum luminance of 1352 cd m^{-2} and EQE of 4.2% emitted pure white light.

5.2.2 Surface chemistry engineering. In addition to the factors aforementioned, QDs are mostly modified by long-chain organic ligands (such as oleic acid and oleamine), which hinder the charge injection between the transport layer and the emission layer. As a result, internal charge carrier transport progress becomes weak, which seriously affects the efficiency of the devices. One method to solve this problem is to replace the long-chain ligands with short ones. Ji *et al.*[94] replaced the oleic acid with a shorter ligand 1,2-ethanedithiol and the as-prepared AIS QDs were used as the emitting layer to fabricate QLEDs. They showed that the treated QD layers became more compact and smoother, while the film mobility also increased. The EQE of this QLED was 1.52%, higher than those of the device employing original AIS QDs (EQE of 0.026%). Wang *et al.*[95] considered that proton transfer between different kinds of ligands binding to the surface would decrease the stability and efficiency of QLEDs and a synthesis method using a single ligand can fix this issue. They demonstrated the synthesis of CIS/ZnS QDs using 1-dodecanethiol as the single solvent, the S source, and the capping ligand. They confirmed that the coating of the ZnS shell could strip off the long carbon chains originally on the surface of CIS QDs, which contributed to the surface modification in further LED fabrication (Fig. 11). After replacing the long-chain $[Mim]BF_4$ with short-chain 1,2-ethanedithiol (EDT), they fabricated a QLED using the as-synthesized CIS/ZnS QDs. The QLED showed an EQE of 7.8%, the highest value among the QLEDs based on CIS QDs.

5.2.3 Emitter selection engineering. The early white QLEDs mainly used inorganic/organic composite materials. I–III–VI QDs provide the red or yellow component of white light, while the blue or green color comes from organic emitters. Liu *et al.*[96] reported a white QLED containing a mixture of yellow emissive ZCIS/ZnS QDs and blue emissive poly [(9,9-dioctylfluorenyl-2,7-diyl)-*co*-(4,4′-(*N*-(*p*-butylphenyl)) diphenylamine)] (TFB) as a single emissive layer. This QLED showed a low turn-on voltage of 2.5 V and a maximum luminance of 1500 cd m^{-2}. However, organic polymers are relatively easy to degrade, which may result in shorter lifetimes and stronger emission color instability. Employing QDs as emitters solely has become a trend. Yoon and coworkers[97] fabricated white QLEDs in which the blue ZnCuGaS (ZCGS) QDs blending with the yellow CIS QDs were used as emissive layers (Fig. 12). At the best ZCGS-to-CIS QD content ratio, the QLED displayed a CRI of 82, a maximum luminance of 2172 cd m^{-2}, and an EQE of 4.6%. Furthermore, using single-component QDs as white EML rather than multiple QDs of different colors can be highly advantageous because it can improve bias-insensitive color stability and facilitate device fabrication. Zhang *et al.*[98] implemented white-light-emitting Ag, Mn: ZnGaS/ZnS QDs with a PL QY up to 90% to fabricate QLEDs composed of ITO/ZnO/QDs/PEIE/poly-TPD/PMAH/Al. The EL spectrum of the device was composed of three spectral emission bands corresponding to poly-TPD, Ag^+ dopant, and Mn^{2+} dopant. The maximum luminance was 6.5 cd m^{-2}.

6. Conclusions

In this review, we have summarized the synthesis methods of I–III–VI QDs in the organic and aqueous phase and introduced their structure with respect to doping, alloying and core–shell. Furthermore, special focus has been paid to their applications in photoluminescent and electroluminescent WLEDs. I–III–VI

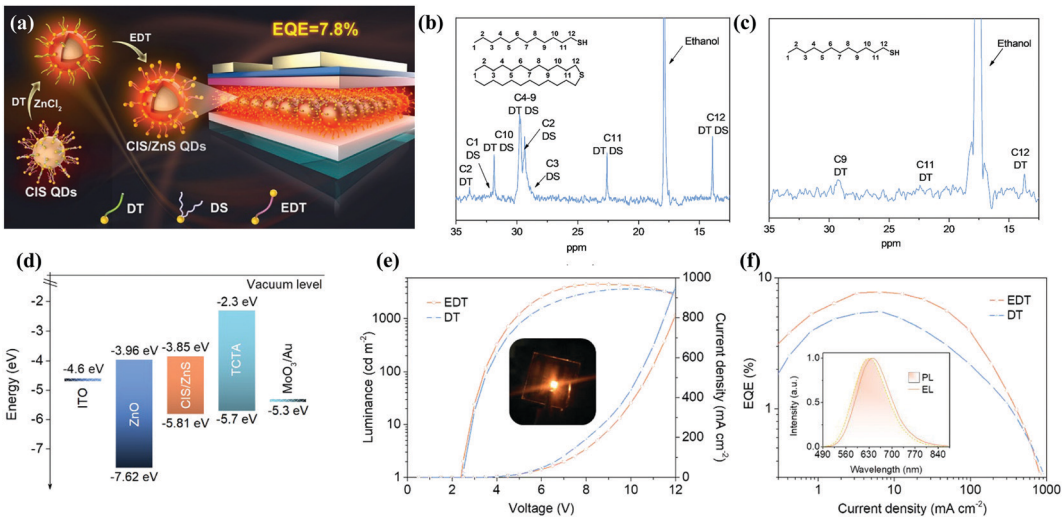

Fig. 11 (a) Schematic illustration of the synthesis procedures of CIS/ZnS QDs and the structure of the multilayered QLED. ^{13}C NMR spectra of (b) CIS core QDs and (c) CIS/ZnS core/shell QDs in $CDCl_3$. (d) Energy band diagram of an inverted LED structure. Driving voltage-dependent (e) current density and brightness evolution of the QLEDs and a photograph of the operating device (inset). Current density-dependent (f) EQE evolution and normalized device PL and EL spectra (inset) of the QLEDs. Reproduced with permission.[95] Copyright 2018, American Chemical Society.

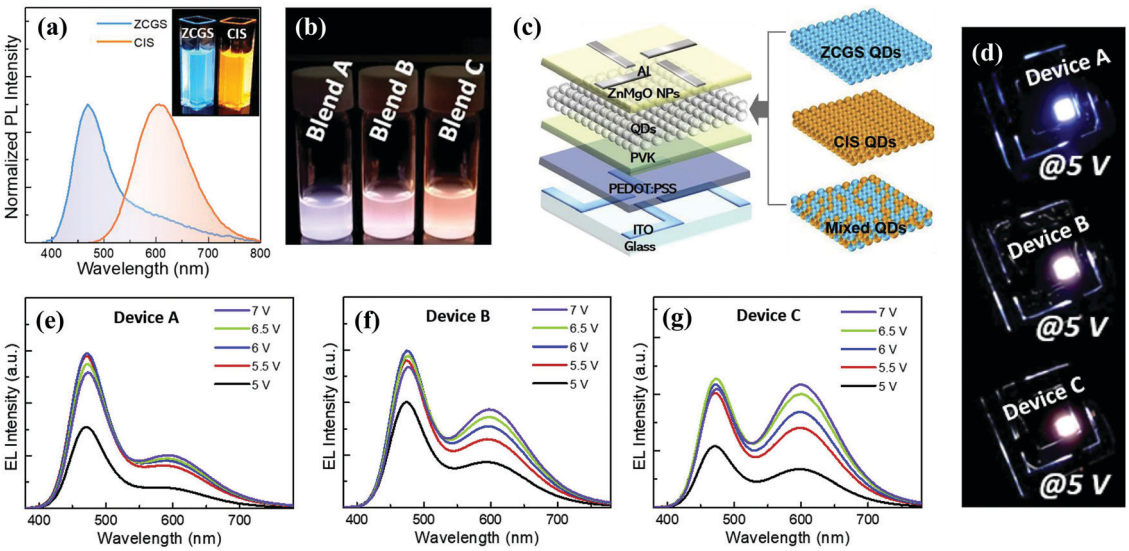

Fig. 12 (a) Normalized PL spectra of ZCGS/ZnS and CIS/ZnS QDs. (b) Photograph of three QD blend solutions with different ZCGS/CIS QD weight ratios under UV irradiation. (c) Schematic structure of multilayered QLED with different EMLs of blue ZCGS, yellow CIS QDs, and their mixture. (d) Representative EL images of three bicolored white QLEDs based on blend A, B, and C. Voltage-dependent EL spectral evolutions of three bicolored white QLEDs of device (e) A, (f) B, and (g) C. Reproduced with permission.[97] Copyright 2019 Elsevier Ltd. All rights reserved.

QDs have attracted huge interest from researchers due to their unique properties, such as large Stokes shift, wide emission bandwidth, and good tunability, which make them promising candidates in WLEDs. Despite these superiorities, there are still some challenges in their preparation and application as follows.

First, most of the high-quality I–III–VI QDs reported recently have been synthesized *via* organic methods, which require strict experimental conditions, need a relatively complex operation, and do harm to the environment, while the PL QYs of QDs synthesized in the aqueous phase are relatively low. The development of new synthetic technologies is particularly important.

Second, the properties of I–III–VI QDs cannot be precisely designed due to their complex composition. At present, the luminous mechanism of I–III–VI QDs is controversial, and further study of the mechanism can guide the synthesis of high-quality QDs. In addition, more attention should be paid to the structural design of I–III–VI QDs. At present, the structural design of QDs is empirical and has great uncertainty. There is still a need to distinguish the optimum synthetic parameters for synthesizing doped or alloyed nanocrystals. The ability to precisely control the shell thickness and the degree of alloying will greatly promote the synthesis and application of I–III–VI QDs in various fields.

Third, when I–III–VI QDs are used as the conversion layer of WLEDs, thermal degradation will affect both the QDs and packaging matrices, resulting in optical attenuation and other adverse effects. Therefore, it is particularly critical to improve the structure of QD-LEDs and choose matrix materials with better compatibility and thermal stability. Additionally, the EQE, LE, and other parameters of I–III–VI QD-based EL devices are still far from those based on Cd-containing or perovskite QDs.[99,100] It is necessary to study the working mechanism of the devices further and design the structure of each functional layer reasonably to realize the charge injection balance. In addition, it is also crucial to design the structure of QDs.

Despite these challenges, I–III–VI QDs are still expected to be promising materials for low-cost and high-performance WLEDs. Further extensive research and development efforts should be devoted to overcoming the problems aforementioned and thus contributing to future commercialization.

Author contributions

Hanxu Lu: Methodology, investigation, writing – original draft. Zhe Hu: methodology, investigation, writing – original draft. Wenjie Zhou: writing – review & editing, formal analysis. Jinxin Wei: writing – review & editing. Wanlu Zhang: supervision. Fengxian Xie: supervision, project administration. Ruiqian Guo: supervision, project administration, funding acquisition.

Conflicts of interest

There are no conflicts to declare.

Acknowledgements

This work was supported by the National Natural Science Foundation of China (NSFC, No. 62074044 and NSFC, No. 61904036), the Zhongshan – Fudan Joint Innovation Center and Jihua Laboratory Projects of Guangdong Province (X190111UZ190).

Notes and references

1 Z. Liu, C. H. Lin, B. R. Hyun, C. W. Sher, Z. Lv, B. Luo, F. Jiang, T. Wu, C. H. Ho, H. C. Kuo and J. H. He, Micro-light-emitting diodes with quantum dots in display technology, *Light: Sci. Appl.*, 2020, **9**, 83.
2 H. Zhang, H. Zhang, A. Pan, B. Yang, L. He and Y. Wu, Rare Earth-Free Luminescent Materials for WLEDs: Recent Progress and Perspectives, *Adv. Mater. Technol.*, 2020, **6**, 2000648.
3 E. Nannen, J. Frohleiks and S. Gellner, Light-Emitting Electrochemical Cells Based on Color-Tunable Inorganic Colloidal Quantum Dots, *Adv. Funct. Mater.*, 2020, **30**, 1907349.
4 H. Zhang, W. Fang, Y. Zhong and Q. Zhao, Zn–Ag–In–S quantum dot sensitized solar cells with enhanced efficiency by tuning defects, *J. Colloid Interface Sci.*, 2019, **547**, 267–274.
5 H. Song, Y. Lin, M. Zhou, H. Rao, Z. Pan and X. Zhong, Zn–Cu–In–S–Se Quinary "Green" Alloyed Quantum-Dot-Sensitized Solar Cells with a Certified Efficiency of 14.4, *Angew. Chem., Int. Ed.*, 2021, **60**, 6137–6144.
6 R. Zhang, T. Deng, J. Wang, G. Wu, S. Li, Y. Gu and D. Deng, Organic-to-aqueous phase transfer of Zn–Cu–In–Se/ZnS quantum dots with multifunctional multidentate polymer ligands for biomedical optical imaging, *New J. Chem.*, 2017, **41**, 5387–5394.
7 T. Kameyama, H. Yamauchi, T. Yamamoto, T. Mizumaki, H. Yukawa, M. Yamamoto, S. Ikeda, T. Uematsu, Y. Baba, S. Kuwabata and T. Torimoto, Tailored Photoluminescence Properties of Ag(In,Ga)Se_2 Quantum Dots for Near-Infrared In Vivo Imaging, *ACS Appl. Nano Mater.*, 2020, **3**, 3275–3287.
8 S. Luo, J. Ke, M. Yuan, Q. Zhang, P. Xie, L. Deng and S. Wang, $CuInS_2$ quantum dots embedded in Bi_2WO_6 nanoflowers for enhanced visible light photocatalytic removal of contaminants, *Appl. Catal., B*, 2018, **221**, 215–222.
9 D. Zhang, B. Mao, D. Li, Y. Liu, F. Li, W. Dong, T. Jiang and W. Shi, 0D/2D Z-scheme heterojunctions of Zn-$AgIn_5S_8$ QDs/α-Fe_2O_3 nanosheets for efficient visible-light-driven hydrogen production, *Chem. Eng. J.*, 2021, **417**, 128275.
10 J. Wei, Z. Hu, W. Zhou, Y. Qiu, H. Dai, Y. Chen, Z. Cui, S. Liu, H. He, W. Zhang, F. Xie and R. Guo, Emission tuning of highly efficient quaternary Ag-Cu-Ga-Se/ZnSe quantum dots for white light-emitting diodes, *J. Colloid Interface Sci.*, 2021, **602**, 307–315.
11 Z. Bai, W. Ji, D. Han, L. Chen, B. Chen, H. Shen, B. Zou and H. Zhong, Hydroxyl-Terminated $CuInS_2$ Based Quantum Dots: Toward Efficient and Bright Light Emitting Diodes, *Chem. Mater.*, 2016, **28**, 1085–1091.
12 K. Bourzac, Quantum dots go on display, *Nature*, 2013, **493**, 283.
13 S.-R. Chung, C.-B. Siao and K.-W. Wang, Full color display fabricated by CdSe bi-color quantum dots-based white light-emitting diodes, *Opt. Mater. Express*, 2018, **8**, 2677.
14 S. Tamang, C. Lincheneau, Y. Hermans, S. Jeong and P. Reiss, Chemistry of InP Nanocrystal Syntheses, *Chem. Mater.*, 2016, **28**, 2491–2506.
15 H. B. Chandrasiri, E. B. Kim and P. T. Snee, Sterically Encumbered Tris(trialkylsilyl) Phosphine Precursors for Quantum Dot Synthesis, *Inorg. Chem.*, 2020, **59**, 15928–15935.
16 S. Jain, S. Bharti, G. K. Bhullar and S. K. Tripathi, I–III–VI core/shell QDs: Synthesis, characterizations and applications, *J. Lumin.*, 2020, **219**, 116912.
17 O. Yarema, M. Yarema and V. Wood, Tuning the Composition of Multicomponent Semiconductor Nanocrystals: The Case of I–III–VI Materials, *Chem. Mater.*, 2018, **30**, 1446–1461.
18 S. Palchoudhury, K. Ramasamy and A. Gupta, Multinary copper-based chalcogenide nanocrystal systems from the perspective of device applications, *Nanoscale Adv.*, 2020, **2**, 3069–3082.
19 S. Li, X. Tang, Z. Zang, Y. Yao, Z. Yao, H. Zhong and B. Chen, I–III–VI chalcogenide semiconductor nanocrystals: Synthesis, properties, and applications, *Chin. J. Catal.*, 2018, **39**, 590–605.

20 J. McKittrick, L. E. Shea-Rohwer and D. J. Green, Review: Down Conversion Materials for Solid-State Lighting, *J. Am. Ceram. Soc.*, 2014, **97**, 1327–1352.
21 H. Zhong, Z. Bai and B. Zou, Tuning the Luminescence Properties of Colloidal I–III–VI Semiconductor Nanocrystals for Optoelectronics and Biotechnology Applications, *J. Phys. Chem. Lett.*, 2012, **3**, 3167–3175.
22 S. L. Castro, S. G. Bailey, R. P. Raffaelle, K. K. Banger and A. F. Hepp, Synthesis and Characterization of Colloidal $CuInS_2$ Nanoparticles from a Molecular Single-Source Precursor, *J. Phys. Chem. B*, 2004, **108**, 12429–12435.
23 X. Huang, R. Yu, X. Yang, X. Xu, H. Zhang and D. Zhang, Efficient $CuInS_2$/ZnS based quantum dot light emitting diodes by engineering the exciton formation interface, *J. Lumin.*, 2018, **202**, 339–344.
24 W. Xiang, C. Xie, J. Wang, J. Zhong, X. Liang, H. Yang, L. Luo and Z. Chen, Studies on highly luminescent $AgInS_2$ and Ag–Zn–In–S quantum dots, *J. Alloys Compd.*, 2014, **588**, 114–121.
25 O. Stroyuk, A. Raevskaya, F. Spranger, O. Selyshchev, V. Dzhagan, S. Schulze, D. R. T. Zahn and A. Eychmüller, Origin and Dynamics of Highly Efficient Broadband Photoluminescence of Aqueous Glutathione-Capped Size-Selected Ag–In–S Quantum Dots, *J. Phys. Chem. C*, 2018, **122**, 13648–13658.
26 P. Galiyeva, H. Rinnert, L. Balan, H. Alem, G. Medjahdi, B. Uralbekov and R. Schneider, Single-source precursor synthesis of quinary AgInGaZnS QDs with tunable photoluminescence emission, *Appl. Surf. Sci.*, 2021, **562**, 150143.
27 B. Y. Kim, J. H. Kim, K. H. Lee, E. P. Jang, C. Y. Han, J. H. Jo, H. S. Jang and H. Yang, Synthesis of highly efficient azure-to-blue-emitting Zn–Cu–Ga–S quantum dots, *Chem. Commun.*, 2017, **53**, 4088–4091.
28 R. G. Pearson, Hard and Soft Acids and Bases, *J. Am. Chem. Soc.*, 1963, **85**, 3533–3539.
29 R. Xie, M. Rutherford and X. Peng, Formation of High-Quality I–III–VI Semiconductor Nanocrystals by Tuning Relative Reactivity of Cationic Precursors, *J. Am. Chem. Soc.*, 2009, **131**, 5691–5697.
30 H. Zhong, S. S. Lo, T. Mirkovic, Y. Li, Y. Ding, Y. Li and G. D. Scholes, Noninjection Gram-Scale Synthesis of Monodisperse Pyramidal $CuInS_2$ Nanocrystals and Their Size-Dependent Properties, *ACS Nano*, 2010, **4**, 5253–5262.
31 A. Heuer-Jungemann, N. Feliu, I. Bakaimi, M. Hamaly, A. Alkilany, I. Chakraborty, A. Masood, M. F. Casula, A. Kostopoulou, E. Oh, K. Susumu, M. H. Stewart, I. L. Medintz, E. Stratakis, W. J. Parak and A. G. Kanaras, The Role of Ligands in the Chemical Synthesis and Applications of Inorganic Nanoparticles, *Chem. Rev.*, 2019, **119**, 4819–4880.
32 C. Coughlan, M. Ibanez, O. Dobrozhan, A. Singh, A. Cabot and K. M. Ryan, Compound Copper Chalcogenide Nanocrystals, *Chem. Rev.*, 2017, **117**, 5865–6109.
33 W. M. Girma, M. Z. Fahmi, A. Permadi, M. A. Abate and J. Y. Chang, Synthetic strategies and biomedical applications of I–III–VI ternary quantum dots, *J. Mater. Chem. B*, 2017, **5**, 6193–6216.
34 S. S. Chetty, S. Praneetha, K. Govarthanan, R. S. Verma and A. Vadivel Murugan, Noninvasive Tracking and Regenerative Capabilities of Transplanted Human Umbilical Cord-Derived Mesenchymal Stem Cells Labeled with I–III–IV Semiconducting Nanocrystals in Liver-Injured Living Mice, *ACS Appl. Mater. Interfaces*, 2019, **11**, 8763–8778.
35 J.-Y. Chang, G.-Q. Wang, C.-Y. Cheng, W.-X. Lin and J.-C. Hsu, Strategies for photoluminescence enhancement of $AgInS_2$ quantum dots and their application as bioimaging probes, *J. Mater. Chem.*, 2012, **22**, 10609.
36 X. Tang, W. B. A. Ho and J. M. Xue, Synthesis of Zn-Doped $AgInS_2$ Nanocrystals and Their Fluorescence Properties, *J. Phys. Chem. C*, 2012, **116**, 9769–9773.
37 C. B. Murray, D. J. Norris and M. G. Bawendi, Synthesis and Characterization of Nearly Monodisperse CdE(E = S, Se, Te) Semiconductor Nanocrystallites, *J. Am. Chem. Soc.*, 1993, **115**, 8706–8715.
38 J. H. Kim, D. Y. Jo, K. H. Lee, E. P. Jang, C. Y. Han, J. H. Jo and H. Yang, White Electroluminescent Lighting Device Based on a Single Quantum Dot Emitter, *Adv. Mater.*, 2016, **28**, 5093–5098.
39 B. Deng, Y. Zhu, J. Li, X. Chen, K. He, J. Yang, K. Qin, Z. Bi, X. Xiao, S. Chen, X. Xu and G. Xu, Low temperature synthesis of highly bright green emission $CuInS_2$/ZnS quantum dots and its application in light-emitting diodes, *J. Alloys Compd.*, 2021, **851**, 155439.
40 S. Mei, G. Zhang, W. Yang, X. Wei, W. Zhang, J. Zhu and R. Guo, A facile route for highly efficient color-tunable Cu–Ga–Se/ZnSe quantum dots, *Appl. Surf. Sci.*, 2018, **456**, 876–881.
41 W. T. Huang, S. Y. Yoon, B. H. Wu, K. M. Lu, C. M. Lin, H. Yang and R. S. Liu, Ultra-broadband near-infrared emission $CuInS_2$/ZnS quantum dots with high power efficiency and stability for the theranostic applications of mini light-emitting diodes, *Chem. Commun.*, 2020, **56**, 8285–8288.
42 T. Chen, Y. Ren, Y. Xu, W. Jiang, L. Wang, W. Jiang and Z. Xie, Room-temperature ionic-liquid-assisted hydrothermal synthesis of Ag–In–Zn–S quantum dots for WLEDs, *J. Alloys Compd.*, 2021, **858**, 158084.
43 Z. Hu, H. Dai, X. Wei, D. Su, C. Wei, Y. Chen, F. Xie, W. Zhang, R. Guo and S. Qu, 49.25% efficient cyan emissive sulfur dots via a microwave-assisted route, *RSC Adv.*, 2020, **10**, 17266–17269.
44 J. X. Soares, K. D. Wegner, D. S. M. Ribeiro, A. Melo, I. Häusler, J. L. M. Santos and U. Resch-Genger, Rationally designed synthesis of bright $AgInS_2$/ZnS quantum dots with emission control, *Nano Res.*, 2020, **13**, 2438–2450.
45 S. J. Rosenthal, J. McBride, S. J. Pennycook and L. C. Feldman, Synthesis, Surface Studies, Composition and Structural Characterization of CdSe, Core/Shell, and Biologically Active Nanocrystals, *Surf. Sci. Rep.*, 2007, **62**, 111–157.
46 Z. Wu, P. Liu, W. Zhang, K. Wang and X. W. Sun, Development of InP Quantum Dot-Based Light-Emitting Diodes, *ACS Energy Lett.*, 2020, **5**, 1095–1106.
47 T. Torimoto, T. Kameyama and S. Kuwabata, Photofunctional Materials Fabricated with Chalcopyrite-Type

Semiconductor Nanoparticles Composed of $AgInS_2$ and Its Solid Solutions, *J. Phys. Chem. Lett.*, 2014, **5**, 336–347.
48 Y. Hamanaka, T. Ogawa, M. Tsuzuki and T. Kuzuya, Photoluminescence Properties and Its Origin of $AgInS_2$ Quantum Dots with Chalcopyrite Structure, *J. Phys. Chem. C*, 2011, **115**, 1786–1792.
49 B. Chen, N. Pradhan and H. Zhong, From Large-Scale Synthesis to Lighting Device Applications of Ternary I–III–VI Semiconductor Nanocrystals: Inspiring Greener Material Emitters, *J. Phys. Chem. Lett.*, 2018, **9**, 435–445.
50 Z. Long, W. Zhang, J. Tian, G. Chen, Y. Liu and R. Liu, Recent research on the luminous mechanism, synthetic strategies, and applications of $CuInS_2$ quantum dots, *Inorg. Chem. Front.*, 2021, **8**, 880–897.
51 I. T. Kraatz, M. Booth, B. J. Whitaker, M. G. D. Nix and K. Critchley, Sub-Bandgap Emission and Intraband Defect-Related Excited-State Dynamics in Colloidal $CuInS_2$/ZnS Quantum Dots Revealed by Femtosecond Pump-Dump-Probe Spectroscopy, *J. Phys. Chem. C*, 2014, **118**, 24102–24109.
52 B. Chen, H. Zhong, W. Zhang, Z. A. Tan, Y. Li, C. Yu, T. Zhai, Y. Bando, S. Yang and B. Zou, Highly Emissive and Color-Tunable $CuInS_2$-Based Colloidal Semiconductor Nanocrystals: Off-Stoichiometry Effects and Improved Electroluminescence Performance, *Adv. Funct. Mater.*, 2012, **22**, 2081–2088.
53 H. Zang, H. Li, N. S. Makarov, K. A. Velizhanin, K. Wu, Y. S. Park and V. I. Klimov, Thick-Shell $CuInS_2$/ZnS Quantum Dots with Suppressed "Blinking" and Narrow Single-Particle Emission Line Widths, *Nano Lett.*, 2017, **17**, 1787–1795.
54 W. van der Stam, M. de Graaf, S. Gudjonsdottir, J. J. Geuchies, J. J. Dijkema, N. Kirkwood, W. H. Evers, A. Longo and A. J. Houtepen, Tuning and Probing the Distribution of Cu^+ and Cu^{2+} Trap States Responsible for Broad-Band Photoluminescence in $CuInS_2$ Nanocrystals, *ACS Nano*, 2018, **12**, 11244–11253.
55 K. E. Knowles, K. H. Hartstein, T. B. Kilburn, A. Marchioro, H. D. Nelson, P. J. Whitham and D. R. Gamelin, Luminescent Colloidal Semiconductor Nanocrystals Containing Copper: Synthesis, Photophysics, and Applications, *Chem. Rev.*, 2016, **116**, 10820–10851.
56 S. Paderick, M. Kessler, T. J. Hurlburt and S. M. Hughes, Synthesis and characterization of $AgGaS_2$ nanoparticles: a study of growth and fluorescence, *Chem. Commun.*, 2017, **54**, 62–65.
57 T. Kameyama, M. Kishi, C. Miyamae, D. K. Sharma, S. Hirata, T. Yamamoto, T. Uematsu, M. Vacha, S. Kuwabata and T. Torimoto, Wavelength-Tunable Band-Edge Photoluminescence of Nonstoichiometric Ag–In–S Nanoparticles *via* Ga^{3+} Doping, *ACS Appl. Mater. Interfaces*, 2018, **10**, 42844–42855.
58 J.-H. Kim, K.-H. Lee, D.-Y. Jo, Y. Lee, J. Y. Hwang and H. Yang, Cu–In–Ga–S quantum dot composition-dependent device performance of electrically driven light-emitting diodes, *Appl. Phys. Lett.*, 2014, **105**, 133104.
59 J.-H. Kim, B.-Y. Kim, E.-P. Jang, S.-Y. Yoon, K.-H. Kim, Y. R. Do and H. Yang, Synthesis of widely emission-tunable Ag–Ga–S and its quaternary derivative quantum dots, *Chem. Eng. J.*, 2018, **347**, 791–797.
60 J.-H. Kim, B.-Y. Kim and H. Yang, Synthesis of Mn-doped $CuGaS_2$ quantum dots and their application as single downconverters for high-color rendering solid-state lighting devices, *Opt. Mater. Express*, 2018, **8**, 221.
61 M. Li, X. Wei, S. Mei, Z. Cui, Y. Fan, B. Yang, Z. Wen, Z. Xiong, L. Wang, F. Xie, W. Zhang and R. Guo, Highly luminescent copper gallium selenium based multicomponent quantum dots: formation process and tunable white-light emission, *Appl. Surf. Sci.*, 2021, **538**, 147907.
62 O. Yarema, M. Yarema, W. M. Lin and V. Wood, Cu–In–Te and Ag–In–Te colloidal nanocrystals with tunable composition and size, *Chem. Commun.*, 2016, **52**, 10878–10881.
63 O. Yarema, M. Yarema, D. Bozyigit, W. M. Lin and V. Wood, Independent Composition and Size Control for Highly Luminescent Indium-Rich Silver Indium Selenide Nanocrystals, *ACS Nano*, 2015, **9**, 11134–11142.
64 A. Saha and G. Konstantatos, Ag_2ZnSnS_4–ZnS core–shell colloidal quantum dots: a near-infrared luminescent material based on environmentally friendly elements, *J. Mater. Chem. C*, 2021, **9**, 5682–5688.
65 M. D. Regulacio and M.-Y. Han, Composition-Tunable Alloyed Semiconductor Nanocrystals, *Acc. Chem. Res.*, 2010, **43**, 621–630.
66 J. Hu, J. Song, Z. Tang, H. Li, L. Chen and R. Zhou, Phospholipid-stabilized $Cu_xAg_{1-x}InSe_2$ nanocrystals as luminophores: fabrication, optical properties, and biological application, *J. Mater. Chem. C*, 2020, **8**, 5821–5831.
67 T. Bai, C. Li, F. Li, L. Zhao, Z. Wang, H. Huang, C. Chen, Y. Han, Z. Shi and S. Feng, A simple solution-phase approach to synthesize high quality ternary AgInSe2 and band gap tunable quaternary $AgIn(S_{1-x}Se_x)_2$ nanocrystals, *Nanoscale*, 2014, **6**, 6782–6789.
68 D. Deng, L. Qu, J. Zhang, Y. Ma and Y. Gu, Quaternary Zn–Ag–In–Se quantum dots for biomedical optical imaging of RGD-modified micelles, *ACS Appl. Mater. Interfaces*, 2013, **5**, 10858–10865.
69 B. Bhattacharyya and A. Pandey, $CuFeS_2$ Quantum Dots and Highly Luminescent CuFeS2 Based Core/Shell Structures: Synthesis, Tunability, and Photophysics, *J. Am. Chem. Soc.*, 2016, **138**, 10207–10213.
70 S.-Y. Yoon, J.-H. Kim, E.-P. Jang, S.-H. Lee, D.-Y. Jo, Y. Kim, Y. R. Do and H. Yang, Systematic and Extensive Emission Tuning of Highly Efficient Cu–In–S-Based Quantum Dots from Visible to Near Infrared, *Chem. Mater.*, 2019, **31**, 2627–2634.
71 P. Reiss, M. Protiere and L. Li, Core/Shell semiconductor nanocrystals, *Small*, 2009, **5**, 154–168.
72 T. Pons, E. Pic, N. Lequeux, E. Cassette, L. Bezdetnaya, F. Guillemin, F. Marchal and B. Dubertret, Cadmium-Free $CuInS_2$/ZnS Quantum Dots for Sentinel Lymph Node Imaging with Reduced Toxicity, *ACS Nano*, 2010, **4**, 2531–2538.
73 L. Li, A. Pandey, D. J. Werder, B. P. Khanal, J. M. Pietryga and V. I. Klimov, Efficient synthesis of highly luminescent copper indium sulfide-based core/shell nanocrystals with surprisingly long-lived emission, *J. Am. Chem. Soc.*, 2011, **133**, 1176–1179.

74 J. Feng, M. Sun, F. Yang and X. Yang, A facile approach to synthesize high-quality $Zn_xCu_yInS_{1.5+x+0.5y}$ nanocrystal emitters, *Chem. Commun.*, 2011, **47**, 6422–6424.
75 S. H. Park, A. Hong, J. H. Kim, H. Yang, K. Lee and H. S. Jang, Highly bright yellow-green-emitting $CuInS_2$ colloidal quantum dots with core/shell/shell architecture for white light-emitting diodes, *ACS Appl. Mater. Interfaces*, 2015, **7**, 6764–6771.
76 A. C. Berends, W. van der Stam, J. P. Hofmann, E. Bladt, J. D. Meeldijk, S. Bals and C. de Mello, Donega, Interplay between Surface Chemistry, Precursor Reactivity, and Temperature Determines Outcome of ZnS Shelling Reactions on $CuInS_2$ Nanocrystals, *Chem. Mater.*, 2018, **30**, 2400–2413.
77 Z. Liu, Z. Guan, X. Li, A. Tang and F. Teng, Rational Design and Synthesis of Highly Luminescent Multinary Cu–In–Zn–S Semiconductor Nanocrystals with Tailored Nanostructures, *Adv. Opt. Mater.*, 2020, **8**, 1901555.
78 E. C. Hansen, S. N. Bertram, J. J. Yoo and M. G. Bawendi, Zinc Thiolate Enables Bright Cu-Deficient Cu-In-S/ZnS Quantum Dots, *Small*, 2019, **15**, e1901462.
79 L. Wang, X. Kang and D. Pan, High color rendering index warm white light emitting diodes fabricated from $AgInS_2$/ZnS quantum dot/PVA flexible hybrid films, *Phys. Chem. Chem. Phys.*, 2016, **18**, 31634–31639.
80 S.-Y. Yoon, Y.-H. Kim, D.-Y. Jo, J.-H. Jo, S.-H. Lee, H.-M. Kim, Y. Kim, S.-K. Kim and H. Yang, Efficient synthesis of multinary Zn–Cu–Ga–$Se_{1-x}S_x$ quantum dots as full visible-covering emitters and their tricolored white electroluminescence, *Chem. Eng. J.*, 2021, **410**, 128426.
81 W.-S. Song and H. Yang, Efficient White-Light-Emitting Diodes Fabricated from Highly Fluorescent Copper Indium Sulfide Core/Shell Quantum Dots, *Chem. Mater.*, 2012, **24**, 1961–1967.
82 H. Li, X. Jiang, A. Wang, X. Chu and Z. Du, Simple Synthesis of $CuInS_2$/ZnS Core/Shell Quantum Dots for White Light-Emitting Diodes, *Front. Chem.*, 2020, **8**, 669.
83 T. Chen, X. Hu, Y. Xu, L. Wang, W. Jiang, W. Jiang and Z. Xie, Hydrothermal synthesis of highly fluorescent Ag–In–S/ZnS core/shell quantum dots for white light-emitting diodes, *J. Alloys Compd.*, 2019, **804**, 119–127.
84 Z. Hu, H. Dai, W. Zhou, J. Wei, H. Zhang, Z. Ye, Y. Qiu, Y. Chen, Z. Duan, J. Wang, W. Zhang, F. Xie and R. Guo, Corrosion resistant solid-state carbon dots@silicalite-1 composite for latent fingerprints detection, *J. Alloys Compd.*, 2022, **889**, 161660.
85 D. Su, L. Wang, M. Li, S. Mei, X. Wei, H. Dai, Z. Hu, F. Xie and R. Guo, Highly luminescent water-soluble $AgInS_2$/ZnS quantum dots-hydrogel composites for warm white LEDs, *J. Alloys Compd.*, 2020, **824**, 153896.
86 J.-H. Kim, B.-Y. Kim, E.-P. Jang, C.-Y. Han, J.-H. Jo, Y. R. Do and H. Yang, A near-ideal color rendering white solid-state lighting device copackaged with two color-separated Cu–X–S (X = Ga, In) quantum dot emitters, *J. Mater. Chem. C*, 2017, **5**, 6755–6761.
87 K. Gugula, M. Entrup, L. Stegemann, S. Seidel, R. Pottgen, C. A. Strassert and M. Bredol, Solid Solution Quantum Dots with Tunable Dual or Ultrabroadband Emission for LEDs, *ACS Appl. Mater. Interfaces*, 2017, **9**, 521–528.
88 Q. Yuan, T. Wang, P. Yu, H. Zhang, H. Zhang and W. Ji, A review on the electroluminescence properties of quantum-dot light-emitting diodes, *Org. Electron.*, 2021, **90**, 106086.
89 C.-Y. Han and H. Yang, Development of Colloidal Quantum Dots for Electrically Driven Light-Emitting Devices, *J. Korean Ceram. Soc.*, 2017, **54**, 449–469.
90 C. Y. Han, S. Y. Yoon, S. H. Lee, S. W. Song, D. Y. Jo, J. H. Jo, H. M. Kim, H. S. Kim and H. Yang, High-performance tricolored white lighting electroluminescent devices integrated with environmentally benign quantum dots, *Nanoscale Horiz.*, 2021, **6**, 168–176.
91 K. H. Lee, J. H. Lee, H. D. Kang, B. Park, Y. Kwon, H. Ko, C. Lee, J. Lee and H. Yang, Over 40 cd A^{-1} Efficient Green Quantum Dot Electroluminescent Device Comprising Uniquely Large-Sized Quantum Dots, *ACS Nano*, 2014, **8**, 4893–4901.
92 J.-H. Kim and H. Yang, High-Efficiency Cu–In–S Quantum-Dot-Light-Emitting Device Exceeding 7%, *Chem. Mater.*, 2016, **28**, 6329–6335.
93 J. H. Kim, K. H. Kim, S. Y. Yoon, Y. Kim, S. H. Lee, H. S. Kim and H. Yang, Tunable Emission of Bluish Zn–Cu–Ga–S Quantum Dots by Mn Doping and Their Electroluminescence, *ACS Appl. Mater. Interfaces*, 2019, **11**, 8250–8257.
94 C. Ji, M. Lu, H. Wu, X. Zhang, X. Shen, X. Wang, Y. Zhang, Y. Wang and W. W. Yu, 1,2-Ethanedithiol Treatment for $AgIn_5S_8$/ZnS Quantum Dot Light-Emitting Diodes with High Brightness, *ACS Appl. Mater. Interfaces*, 2017, **9**, 8187–8193.
95 Z. Wang, X. Zhang, W. Xin, D. Yao, Y. Liu, L. Zhang, W. Liu, W. Zhang, W. Zheng, B. Yang and H. Zhang, Facile Synthesis of Cu–In–S/ZnS Core/Shell Quantum Dots in 1-Dodecanethiol for Efficient Light-Emitting Diodes with an External Quantum Efficiency of 7.8%, *Chem. Mater.*, 2018, **30**, 8939–8947.
96 Z. Liu, A. Tang, Y. Xie, Z. Guan, Y. Chen and F. Teng, Solution-processed planar white light-emitting diodes based on cadmium-free Cu–In–Zn–S/ZnS quantum dots and polymer, *Org. Electron.*, 2017, **45**, 20–25.
97 S.-Y. Yoon, J.-H. Kim, K.-H. Kim, C.-Y. Han, J.-H. Jo, D.-Y. Jo, S. Hong, J. Y. Hwang, Y. R. Do and H. Yang, High-efficiency blue and white electroluminescent devices based on non-Cd IIII–VI quantum dots, *Nano Energy*, 2019, **63**, 103869.
98 W. J. Zhang, C. Y. Pan, F. Cao, H. Wang, Q. Wu and X. Yang, Synthesis and electroluminescence of novel white fluorescence quantum dots based on a Zn–Ga–S host, *Chem. Commun.*, 2019, **55**, 14206–14209.
99 H. Shen, Q. Gao, Y. Zhang, Y. Lin, Q. Lin, Z. Li, L. Chen, Z. Zeng, X. Li, Y. Jia, S. Wang, Z. Du, L. S. Li and Z. Zhang, Visible quantum dot light-emitting diodes with simultaneous high brightness and efficiency, *Nat. Photonics*, 2019, **13**, 192–197.
100 L. Chouhan, S. Ghimire, C. Subrahmanyam, T. Miyasaka and V. Biju, Synthesis, optoelectronic properties and applications of halide perovskites, *Chem. Soc. Rev.*, 2020, **49**, 2869–2885.